Estimating post-depositional detrital remanent magnetization (pDRM) effects for several sediment records using a flexible lock-in function approach

L. Bohsung[1,2], M. Schanner[1,2], M. Korte[1], M. Holschneider[2]

[1]GFZ German Research Centre for Geosciences, Section 2.3, Potsdam, Germany
[2]University of Potsdam, Applied Mathematics, Potsdam, Germany

Key Points:

- We estimate lock-in functions for several sediment records
- We propose a new method to transform relative declinations to absolute values
- The large variety of estimated lock-in functions indicates the importance of taking pDRM distortions into account

Corresponding author: Lukas Bohsung, `lbohsung@gfz-potsdam.de`

Abstract

Geomagnetic field models over past millennia rely on two main data sources: archaeomagnetic data provide snapshots of the geomagnetic field at specific locations, and sediment records deliver time series of the geomagnetic field at specific locations. The limited temporal and spatial coverage of archaeomagnetic data necessitates the incorporation of sediment data especially when models go further back in time. When working with sediment data one should consider the post-depositional detrital remanent magnetization (pDRM) process, which can cause delayed and smoothed signals. To address the distortion associated with the pDRM process a new Bayesian modeling technique incorporating archaeomagnetic data and a class of flexible parameterized lock-in functions has been proposed. In this study, we investigate this method in more detail and apply it to several sediment records. Our data-driven results support the hypothesis that the pDRM process can introduce distortions, including offsets and smoothing, in some sediment records. Additionally, we demonstrate an effective correction approach to minimize the distortion caused by the pDRM process and its impact on geomagnetic field reconstructions. The variability in the results observed across the nine records points to a potential dependence on sedimentological characteristics. To explore this further, we plan to systematically apply our novel method to a larger number of records in future studies.

Plain Language Summary

Understanding the Earth's magnetic field changes over the past millennia helps us learn more about the planet's history. We can use the magnetic field information preserved in different materials to reconstruct the past Earth's magnetic field evolution: ancient artifacts (archaeomagnetic data), lava flows and sediment records. Archaeomagnetic and lava flow data has limited coverage in time and space, so when modeling longer time scales we have to rely more and more on sediment data. When using sediment data, we need to be careful about a process called post-depositional detrital remanent magnetization (pDRM), which can distort the signals and cause smoothing and delays. To deal with this issue, a new method has been developed using Bayesian modeling, archaeomagnetic data and flexible lock-in functions to correct for the pDRM effect. In this study we explore this method in more detail and test it on several sediment records. We found that the pDRM process indeed introduces distortions in several sediment records.

1 Introduction

In recent decades, numerous data-based models of the past geomagnetic field have been developed using various data collections and modeling methods (e.g. Arneitz et al., 2019; Constable et al., 2016; Hellio & Gillet, 2018; Nilsson & Suttie, 2021; Schanner et al., 2022). These models have varying degrees of accuracy and uncertainty and cover different time periods. One valuable data source for models of the geomagnetic field of the past millennia is archaeomagnetic data, but the uneven data coverage limits its usability. Sediment records provide an additional data source that covers larger time periods and improves the spatial coverage.

The magnetization process in sediments is different from that in archaeological materials and lava flows. In archaeological materials and lava flows, thermoremanent magnetization (TRM) occurs when the material cools down from above the Curie temperature (e.g. Stacey, 2012). This is a well-understood process that finishes within hours or weeks, and delivers a valuable snapshot of the geomagnetic field at this point of time.

The magnetization in sediments is called detrital remanent magnetization (DRM), which was first measured by McNish and Johnson (1938). It is affected by various factors, such as the interaction of magnetic particles with the substrate at the sediment-water interface and dewatering of the sediment (Irving, 1957). The terminology and classification of these effects are not consistent in the literature. We will use the terminol-

ogy used in Bohsung et al. (2023) as recommended by Verosub (1977) in a review paper. According to Verosub (1977), DRM refers to the remanent magnetization found in sediments, and depositional DRM (dDRM) describes the magnetization acquired by the interaction of the particles with the substrate at the sediment-water interface. The term post-depositional DRM (pDRM) refers to any magnetization acquired after the particles settled on the sediment-water interface. There are various effects that fall under the term dDRM, such as the inclination error (R. King, 1955) and the distortion of the inclination caused by aligned particles rolling into the nearest depression of the sediment-water interface (Griffiths et al., 1960).

The traditional pDRM model, established through decades of research, initially sees coarse-grained sediments mechanically fixed upon deposition. Smaller particles within water-filled voids or sediment pores remain mobile but gradually become locked as the sediment consolidates (e.g. Irving, 1957; Irving & Major, 1964; Kent, 1973; Hamano, 1980; Otofuji & Sasajima, 1981). However, alternative theories challenge this model, suggesting sediment flocculation limits grain movement (Katari et al., 2000). Bioturbation's role has also led to alternative sediment mixing models (e.g. Egli & Zhao, 2015). In summary, while the precise pDRM processes remain incompletely understood, consensus has emerged that they result in a delayed and smoothed magnetic signal. This signal is represented as the weighted sum of the geomagnetic field over the lock-in time, characterized by the so-called lock-in functions (Roberts & Winklhofer, 2004; Suganuma et al., 2011).

In Bohsung et al. (2023) a new class of flexible lock-in functions capable of modeling the delay and smoothing related to the pDRM process was presented. Depending on four parameters these lock-in functions can approximate a wide range of possible lock-in behaviors. For the estimation of these four parameters a Bayesian modeling technique based on Gaussian Processes and utilizing archaeomagnetic data as a reference was presented in Bohsung et al. (2023). Synthetic tests outlined in Bohsung et al. (2023) demonstrated the effectivity of the proposed method.

In this paper we apply the proposed method to real world sediment records from various globally distributed locations. We focus on sediment records covering Holocene time periods. The utilization of real sediment data necessitates the comprehensive consideration of factors extending beyond the inherent distortions attributed to the pDRM process. Rigorous and careful data selection and preprocessing procedures are crucial. This includes aspects such as estimation of declination offsets, considering inclination shallowing effects, the formulation of a robust age-depth model and the judicious identification and exclusion of outliers. Within the scope of this study, our primary focus remains centered on the comprehensive examination of the pDRM process effects and the newly proposed methodology. Consequently, we handle declination offsets as well as inclination shallowing as a part of the preprocessing procedure.

In section 2 we summarize the method proposed in Bohsung et al. (2023). A list of nine sediment records is presented in section 2.7. The preprocessing of these records includes a new method for estimating the offset required to transferring relative to absolute declinations, as well as the construction of updated age-depth models, using the most recent radiocarbon calibration curves. In section 3 we apply the method to these sediment records and present the results, which then are discussed and interpreted in section 4.

2 Method and Materials

2.1 Geomagnetic Field Model

As in Schanner et al. (2022) and Bohsung et al. (2023) we use a Bayesian approach and describe the geomagnetic field as realization of a Gaussian Process

$$\mathbf{B} \sim \mathcal{GP}(\bar{\mathbf{B}}, K_{\mathbf{B}}) \tag{1}$$

with constant (space, time dependent) mean function $\bar{\mathbf{B}}$ and kernel function $K_{\mathbf{B}}$.

The a priori assumptions are the same as in Bohsung et al. (2023), which are consistent with the estimated hyperparameters given in Table 2 of Schanner et al. (2022). This means that, a priori, all Gauss coefficients are uncorrelated at a reference radius $R = 2800\,\mathrm{km}$ with zero mean except for the axial dipole. For the axial dipole we assume a constant mean value of $\gamma_1^0 = -38\,\mu\mathrm{T}$ (at the Earth's surface). Further, we assume an a priori variance $\alpha_{\mathrm{DP}} = 39\,\mu\mathrm{T}$ for the dipole and an a priori variance $\alpha_{\mathrm{ND}} = 118.22\,\mu\mathrm{T}$ for all higher degrees (at the reference radius). The temporal correlation of the Gauss coefficients are given by

$$\rho_l(\Delta t) = \left(1 + \frac{|\Delta t|}{\tau_l}\right) \mathrm{e}^{-\frac{|\Delta t|}{\tau_l}} \tag{2}$$

where the correlation time is given by $\tau_l = \begin{cases} 171.34\,\mathrm{yrs} & l = 1 \text{ (dipole)} \\ \frac{379.59}{l}\,\mathrm{yrs} & l > 1 \text{ (non-dipole)} \end{cases}$.

As mentioned in Bohsung et al. (2023), these parameters reflect statistical characteristics of archaeomagnetic data and a direct physical interpretation is not obvious. Take, for instance, $\gamma_1^0 = -38\mu\mathrm{T}$; this represents the optimal value when fitting an axial dipole to the data. Correlation times, though potentially linked to physical processes, are essentially derived from variability resolved in the data. Exploring alternative prior parameters is straightforward, and we anticipate conducting a comprehensive exploration of their impact in future investigations.

2.2 Age-Depth Model

Many of the age-depth models published together with the original data do not report uncertainties. Further, most of them are constructed using out-dated calibration curves (i.e. older versions of IntCal, SHCal and/or Marine; see Reimer et al. (2020), Hogg et al. (2020) and Heaton et al. (2020) for the most recent curves). To incorporate uncertainties from the age-depth determination into our modeling, we recalibrate all records based on available radiocarbon ages. Therefore, we pursue an MCMC based approach, similar to the modification of *bacon* (Blaauw & Christen, 2011) that was proposed by Nilsson and Suttie (2021). Due to shifts in the Marine20 curve, some age-depth models deviate by about one hundred years from the originally published ones. However, many original curves already contained an estimation of the local reservoir effect and therefore the shift in Marine20 does not translate to all age-depth models directly. The main benefit of recalibrating the age-depth models is the resulting availability of dating uncertainties for all sediment records included in this study.

2.3 Lock-in Process

In this section we summarize the findings of Bohsung et al. (2023).

As discussed in the introduction, the pDRM or lock-in process can result in an offset and smoothed signal of the geomagnetic field. This means that the magnetic moment of a layer is given by the weighted average of the geomagnetic field signal over the lock-in depth λ

$$\mathbf{M}(z) = \int_0^{\lambda} \mathbf{B}(z - z')F(z')dz' \tag{3}$$

where $\mathbf{M}(z)$ describes the magnetization of the layer at depth z. The weights are given by a lock-in function F. To ensure that the lock-in function can be used for every layer of a sediment record, we refer to the depth and restrict our analysis to the directional components (i.e. declination and inclination). A comprehensive explanation and analysis can be found in Bohsung et al. (2023). In addition, a class of flexible lock-in functions capable of approximating a wide range of possible lock-in behaviors and previously suggested lock-in functions was derived in Bohsung et al. (2023). The class of piecewise

linear parameterized lock-in functions is given as

$$F_{b_1,b_2,b_3,b_4}(z) = \frac{2}{-b_1 - b_2 + b_3 + b_4} \begin{cases} 0 & z \leq b_1 \\ \frac{z-b_1}{b_2-b_1} & b_1 < z \leq b_2 \\ 1 & b_2 < z \leq b_3 \\ \frac{b_4-z}{b_4-b_3} & b_3 < z \leq b_4 \\ 0 & b_4 \leq z \end{cases} \tag{4}$$

Depending on the four parameters $b_1, b_2, b_3, b_4 \in \mathbb{R}_{\geq 0}$ with $b_1 \leq b_2 \leq b_3 \leq b_4$, the parameterized function F_{b_1,b_2,b_3,b_4} can model the offset as well as the smoothing associated to the lock-in process.

2.4 Estimation of the Lock-in Function Parameters

To estimate the parameters $b_1, \ldots, b_4$, we use the Kalman filter (Kalman, 1960) based method described in Bohsung et al. (2023). In this section we will shortly summarize how the method works. For the estimation we perform a type-II maximum likelihood estimation (Rasmussen, 2004). While closed-form marginal likelihood is available for Gaussian processes (Rasmussen, 2004), its numerical evaluation becomes impractical given the extensive archaeomagnetic dataset used. Therefore, we adopt a sequentialized marginal likelihood evaluation inspired by previous works (Baerenzung et al., 2020; Schanner et al., 2022). The marginal likelihood is approximated as a sum over values calculated for individual Kalman filter steps, providing a measure of how well a set of lock-in function parameters describes the post-depositional remanent magnetization (pDRM) process in a sediment record. This estimation leverages global archaeomagnetic and volcanic data as well as data from a single sediment record, focusing on the last eight thousand years due to the temporal distribution of the archaeological dataset.

A notable difference from existing implementations is the incorporation of a modified observation functional (see Bohsung et al. (2023) for details). This modification accommodates cross correlations between the Kalman filter steps resulting from the convolution integral that leads to a delay and smoothing in the measurements.

Choosing a spherical harmonics cutoff degree of $l_{\max} = 8$ and a Kalman filter step size of $\Delta t = 40$yrs strikes a balance between estimation accuracy and computational efficiency. Extensive tests demonstrate that variations in time steps and cutoff degrees minimally impact estimation accuracy while significantly increasing computational time.

To optimize the log-marginal likelihood (log-ml) we use the methodology including the fifty optimization runs outlined in Bohsung et al. (2023), utilizing dlib's LIPO-TR function optimization algorithm (Malherbe & Vayatis, 2017; D. E. King, 2009). However, in contrast to the synthetic tests performed in Bohsung et al. (2023), determining an appropriate upper bound for the parameter estimation for real sediment records is not straightforward a priori. To address this, we initiated the estimation process with an upper bound of 100 cm and performed ten estimations. In cases where the maximal lock-in depths (values of parameter b_4) of these ten estimated lock-in functions are significantly lower than 100 cm, we performed another forty estimations. Conversely, if the estimated lock-in depths are too close to the upper bound we increased the upper bound by 100 cm. This incremental approach is advised to avoid potential issues where the optimizer converges to local optima.

In our parameter estimation process, we are optimizing the log-ml value. Implicitly we derive a global field model based on archaeomagnetic data and data from a single sediment record. For a complete inversion one would need to store intermediate results and ideally apply a smoothing algorithm in order to incorporate full correlations between the individual steps. However, during the parameter estimation process we do not store and develop this model completely as our focus is on finding lock-in function parameters that maximize the log-ml value. In the synthetic tests performed in Bohsung et al. (2023), we assessed the accuracy of our estimated lock-in function by comparing it with the lock-in function used to generate the synthetic data. However, for real data,

an alternative approach is required. To evaluate the effectiveness of the best-estimated lock-in function, we employ these parameters in a full inversion, where intermediate results are stored, and a smoothing algorithm is applied. Subsequently, the smoothing functional is applied to the posterior and the predictions of the smoothed posterior are compared with the sediment observation. This smoothed posterior, referred to as predicted sediment observations, serves as a benchmark, and the closer its alignment with sediment observations, the more accurate the estimated lock-in function.

2.5 Estimation of the Declination Offset

In general, declinations of a sediment record are reported as relative values, primary due to the absence of core orientation during drilling. Different methods have been proposed to estimate the resulting offset (e.g. Nilsson et al., 2014; Panovska et al., 2015). In this paper, we present a new method based on Bayesian statistics, utilizing the global geomagnetic field model ArchKalmag14k (Schanner et al., 2022) as a reference model. In the future, we intend to incorporate the offset parameter for each sediment record as an extra hyperparameter during the inversion process. However, for the current investigation, our primary focus lies in analyzing the lock-in function. Consequently, we have made the decision to estimate the offset parameter as part of the preprocessing phase.

We use the posterior distribution of the ArchKalmag14k model and a Type-II maximum likelihood estimation to estimate the optimal offset. To incorporate prior information about the offset, we assume a univariate normal prior distribution with mean μ_O and variance σ_O^2. Under the assumption that the mean field is an axial dipole, we set μ_O to the mean distance of the observed relative declinations to zero. This helps to guide the estimation process. In order not to constrain the optimization algorithm too strongly, we set $\sigma_O^2 = 180$.

2.6 Data Preprocessing

The data preprocessing procedure for each sediment record follows a standardized approach. Initially, the declination and inclination values for each record were plotted. Outliers and segments exhibiting unusual behavior were identified and excluded as a first step. Notably, certain segments displayed significant increases or decreases in declination or inclination at the beginning or end of a core or sub-section. As the reasons behind these phenomena remain unexplained, such segments were discarded from both inclination and declination. An example can be found in Figure 1. The points with lower opacity at the beginning of the sub-core BIR2-1 show an unusual decrease. They were excluded from further analysis. Also, three data points from BIR2-3 are excluded. The reason for their exclusion is that they are obvious outliers in the declination (not shown here).

Subsequently, the maximum angular deviation (MAD) values were converted to α_{95} values using the method outlined in Khokhlov and Hulot (2016). In cases where the number of demagnetization steps for certain sediment records was unavailable in the associated publications, a default value of four steps was used. For data points with missing MAD values, a default α_{95} value of 7° was assigned. These α_{95} values were then employed to calculate the measurement errors in declination (D) and inclination (I) according to the formulas (Lanos et al., 2005; Suttie & Nilsson, 2019)

$$\alpha_I = \frac{57.3^\circ}{140}\alpha_{95} \qquad \alpha_D = \frac{1}{\cos(I)}\alpha_I \tag{5}$$

For data points where only declination information was available, but inclination data was missing, an approximation method based on the dominance of the geomagnetic field's dipole nature was utilized. The inclination (I) can then be estimated using the formula

$$I \approx \tan^{-1}(2\tan(\text{lat})) \tag{6}$$

where "lat" represents the latitude at the location of the sediment record.

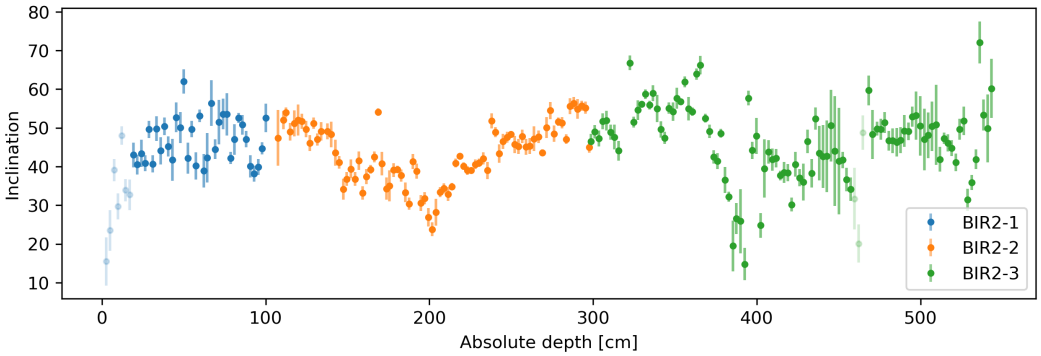

Figure 1. Inclinations of BIR color-coded by its sub-sections. Removed data points are shown with less opacity.

Lastly, the offset parameter, necessary for converting relative declinations into absolute values, was estimated using the methodology proposed in section 2.5.

2.7 Data

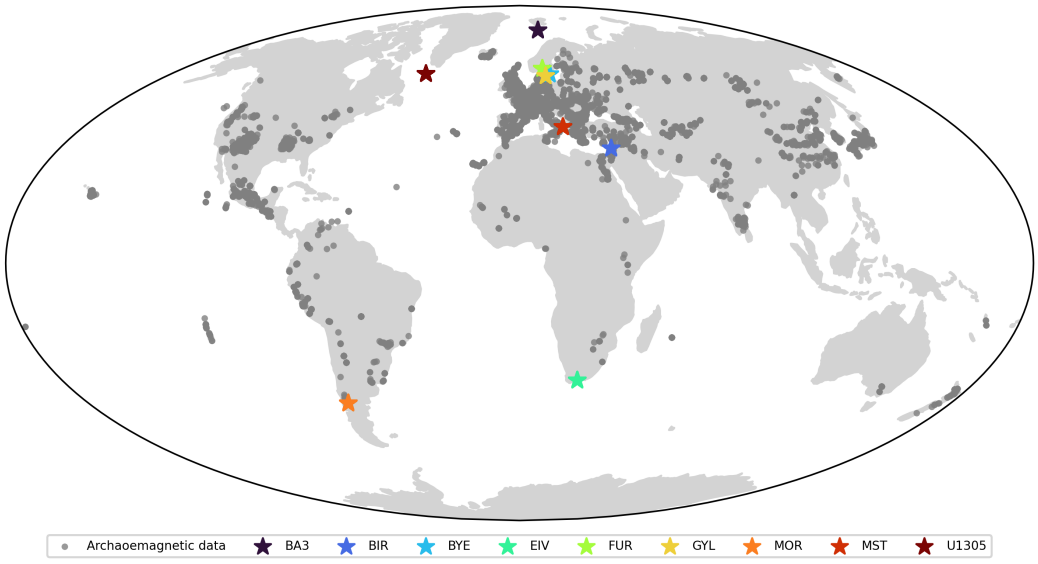

Figure 2. Spatial distribution of used data. Light gray dots represent the archaeomagnetic data and the sediment record locations are represented as colored stars.

We use the same archaeomagnetic data as in Schanner et al. (2022). The spatial distribution is shown in Figure 2 (gray dots).

The proposed method is applied to nine sediment records (see Figure 2 and Table 1). We focus on high quality records, including a good signal without too much noise and reasonable uncertainties. Additionally, we chose sediment records with radiocarbon dating to generate independent age-depth models. In this study we focus on directional data (declination and inclination) only. See Bohsung et al. (2023) for a discussion of this point. In a future study we will investigate the lock-in behavior of intensities and compare it

Table 1. Overview of used sediment records.

Core ID	Sub-cores	Lat (deg)	Long (deg)	N	Time coverage	References	Source
BA3	-	74.850	14.802	434	8585 BC - AD 1496	Caricchi et al. (2018) Caricchi et al. (2020)	GFZ Data Services
BIR	-	33.231	35.769	215	4308 BC - AD 1847	Schwab et al. (2004) Frank et al. (2002) Frank et al. (2003)	Geomagia[1]
BYE	ByaP2, ByaP3	57.383	15.343	284	9263 BC - 75 BC	Snowball and Sandgren (2004)	Geomagia[1]
EIL	-	-33.995	22.640	99	AD 938 - AD 1649	Wündsch et al. (2016)	Pangaea[2] Wündsch et al. (2016)
FUR	P2, P3	59.383	12.080	242	6822 BC - AD 1966	L. Zillén et al. (2003) L. M. Zillén et al. (2002)	Geomagia[1]
GYL	GP1, GP2, GP4	56.759	13.177	419	4494 BC - AD 1178	Mellström et al. (2013) Snowball et al. (2013)	Geomagia[1]
MOR	-	-41.000	288.5	147	10298 BC - AD 1329	Gogorza et al. (2000)	Paper
MST	-	39.834	17.801	138	2009 BC - 477 BC	Béguin et al. (2019)	Author
U1305	-	57.475	311.471	147	6049 BC - AD 1135	Stoner et al. (2013a)	Stoner et al. (2013b)

[1]Brown et al. (2015); [2]Felden et al. (2023).

to the results for directional data. Detailed information about the individual sediment records and especially about their preprocessing is given in section 3.

3 Results

In this section we present the results obtained from estimating the lock-in function parameters. Each sediment record is analyzed individually, and the results are separately visualized in Figures 3-6 and 8 as well as in Figures S1 - S11. These figures provide the following information.

The fifty estimated lock-in functions are visualized in (**A**). The lock-in function with the highest (best) log-ml value is highlighted in orange and was used for the inversion. The remaining estimated lock-in functions are color-coded, ranging from red (indicating a low log-ml value) to blue (indicating a high log-ml value). The distribution of the log-ml values is illustrated in (**D**). To assess the accuracy of our predictions, we present the predicted sediment observations (mean and one hundred samples) for declination and inclination in the upper and lower panels of (**B**), respectively. These predictions are derived from the posterior, generated using the lock-in function highlighted in orange. Furthermore, the directional palaeomagnetic records are shown along with their respective measurement errors. In cases where a sediment record consist of multiple sub-cores or sub-segments we distinguish them by different colors. Additionally, the posterior mean and uncertainties of ArchKalmag14k.r is visualized in gray. To examine the characteristics of the lock-in functions, we employ density plots in (**E**) to (**G**), which demonstrate the distributions of three parameters: half lock-in depth, lock-in function height, and lock-in function width, as described in Bohsung et al. (2023). The density estimation is conducted using Gaussian kernel density estimation. The parameter associated with the lock-in function that yields the best log-ml value is highlighted in orange. Finally, (**C**) shows the mean (red) and fifty samples (gray) of the age-depth model. Radiocarbon ages are depicted as violin plots. The color of the violins indicates which type of calibration curve was used for the individual ages, blue corresponding to the marine and orange to the respective land curve. In most cases the decision which type of curve to use for which radiocarbon sample was guided by the original publication, with bulk sediments being calibrated by the marine curve and plant or wood remanents by the land curves.

Sediment records BYE, FUR and GYL consist of at least two different sub-cores. For each of them we applied the proposed method not only to the combined records but also to the individual sub-cores.

In the following we will present the results for BA3 and BYE. For the results of the remaining records see Supporting Information.

3.1 BA3

Removed data points: Due to an abrupt change observed at a depth of 481 cm, as well as unusual variations in the declination, all data points below this depth were excluded from further analysis.

Declination offset: The sediment record was divided into two sub-sections, namely GEO17603-3-1, which covers the upper part of the record down to a depth of 83 cm, and GEO17603-3-2, which covers the lower part. The estimated declination offset values are -2.46 ± 0.39 for GEO17603-3-1 and -26.04 ± 0.57 for GEO17603-3-2.

Age-depth model: ^{14}C ages were taken from the original publication, table 3. All samples were calibrated using Marine20. See Figure 3 plot (**C**) for the resulting age-depth model.

Estimation: The estimation was performed using an upper bound of 100 cm. Parameter b_4 is significantly lower compared to this upper bound across all fifty estimated lock-in functions, indicating that the chosen bound of 100 cm was appropriate. Furthermore, the predicted sediment observations demonstrated a strong correspon-

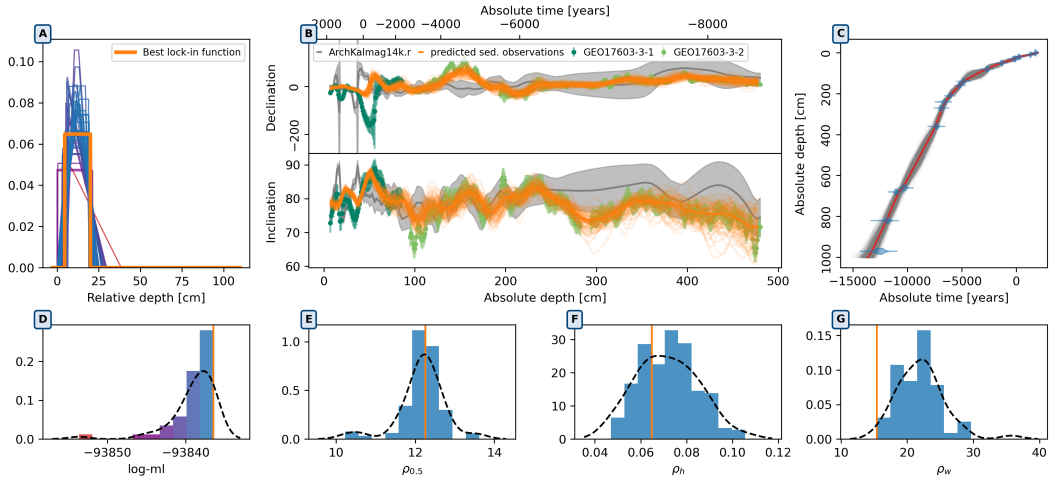

Figure 3. Results for BA3. (**A**) Fifty estimated lock-in functions, with the lock-in function yielding the highest log-ml value highlighted in orange and used for inversion. The remaining functions are color-coded, ranging from red (low log-ml value) to blue (high log-ml value), as illustrated in (**D**). To assess prediction accuracy, we show the mean (thick orange line) and one hundred samples (thin orange lines) of predicted sediment observations for declination and inclination in upper and lower panel of (**B**), derived from the posterior using the orange lock-in function. The directional palaeomagnetic records, along with their respective measurement errors, are depicted, in shades of green distinguishing sub-cores or sub-segments. The gray visualization shows the posterior mean (solid line) and uncertainties (gray area) of ArchKalmag14k.r. (**E**) to (**G**) Density plots of three lock-in function parameters: $\rho_{0.5}, \rho_h$, and ρ_w, respectively. The parameter with the best log-ml value is highlighted in orange. (**C**) Mean (red) and fifty samples (gray) of the age-depth model, with radiocarbon ages depicted as violin plots, color-coded by the type of calibration curve used (blue for marine and orange for land curves).

dence with the actual data, indicating a good fit. Results are visualized in Figure 3.

3.2 BYE

Removed data points: The first 14 data points from the upper part of the sub-core ByaP2 have been removed due to an abrupt decrease in declination.

Declination offset: For the sub-core ByaP2 we estimated an offset of -1.18 ± 0.9 and for ByaP3 an offset of -0.08 ± 1.02.

Age-depth model: ^{14}C ages were taken from the original publication, table 1. All samples were calibrated using IntCal20.

Estimation combined record: Firstly, we conducted ten estimations using an upper bound of 100 cm. Since the parameter values b_4 were too close to this upper bound we decided to increase it to 200 cm. With this new upper bound all parameters b_4 were found to be significantly lower than 200 cm, indicating that this revised upper bound was appropriate. The predicted sediment observations demonstrated a strong correspondence with the declination. Except for the interval between 450 cm and 530 cm, the predicted sediment observations also aligned well with the inclination.

Estimation sub-cores: We can observe a strong agreement in the results obtained for the two sub-cores (ByaP2 and ByaP3, compare Figure 5 and Figure 6) and the

combined data (BYE, see Figure 4). Remarkably, the comparison of the three parameters ($\rho_{0.5}, \rho_h, \rho_w$) derived from the best estimated lock-in functions reveals that the combined record's values fall within the range delineated by the corresponding values of the two sub-cores. These observations indicate a consistent signal in the individual sub-cores and the combined record.

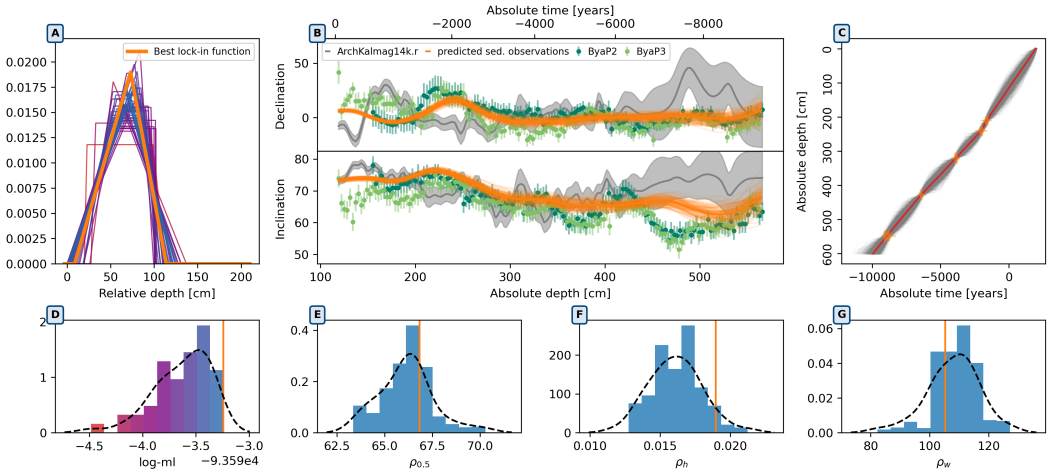

Figure 4. Results for BYE.

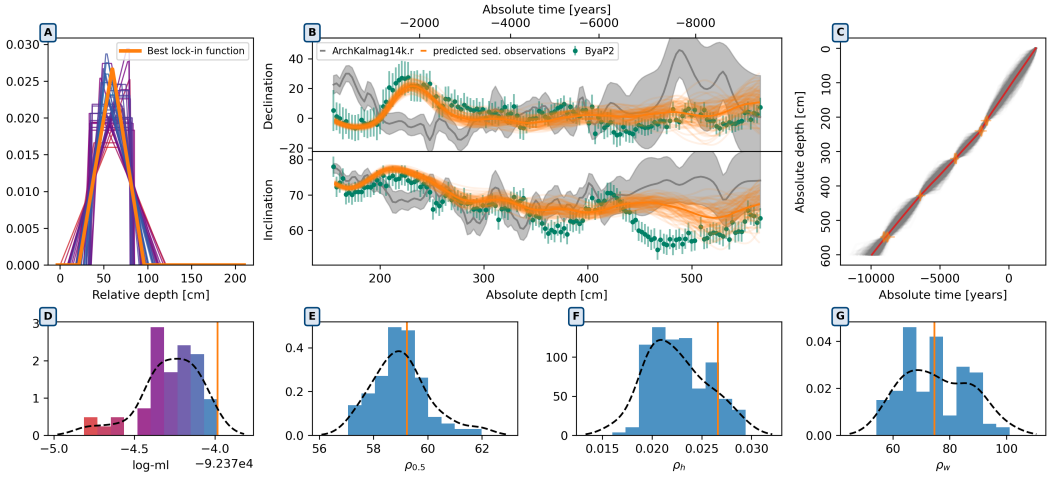

Figure 5. Results for ByaP2.

For more examples see Supporting Information.

The comprehensive results for each record are listed in Table 2. This table not only details the lock-in function parameters —$\rho_{0.5}$, ρ_h, and ρ_w— but also encompasses essential sedimentological aspects of each record. These aspects include the nature of the sediment (freshwater or marine), the water depth at which the sediment was collected, and the derived accumulation rates from the newly generated age-depth models. Additionally, we include some lithostratigraphic information. It's important to note that this summary provides a small snapshot of the data; it extracts only a fraction of the information available in the original publications. For a more in-depth understanding and com-

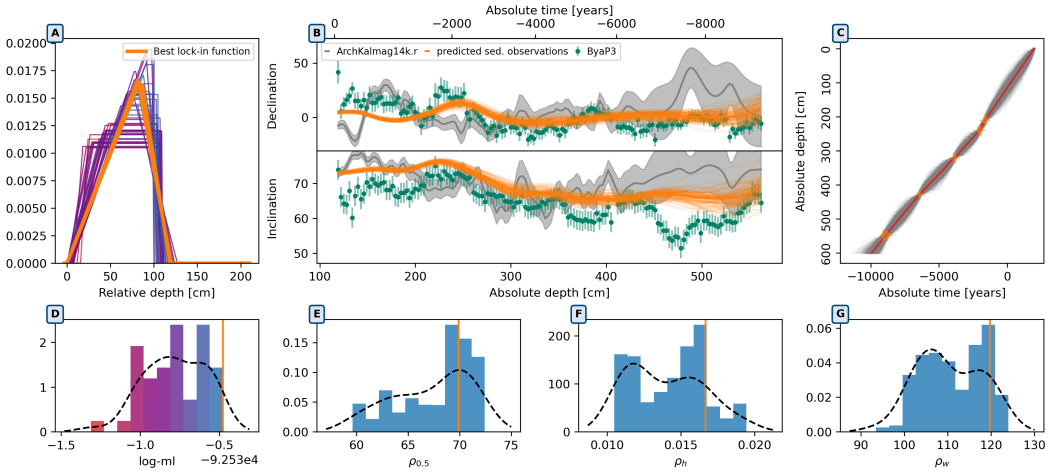

Figure 6. Results for ByaP3.

prehensive data, readers are encouraged to refer to the original publications associated with each record.

3.3 Importance of Data Preprocessing

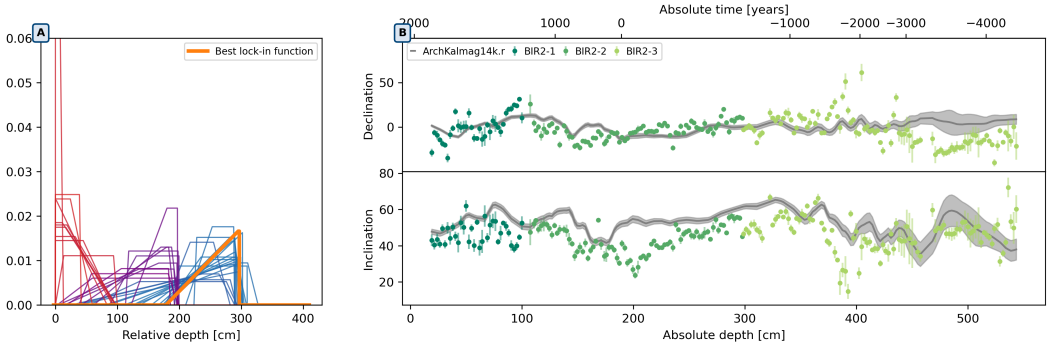

Figure 7. Results for BIR before accounting for inclination shallowing.

In this section we emphasize the importance of proper data preprocessing and data quality verification. We demonstrate the importance using the BIR record as an example. Panel one and two in (**B**) of Figure 7 display declination and inclination of BIR after applying our standard preprocessing procedure (see section 2.6). The estimated lock-in functions after applying our method to the BIR dataset are presented in panel (**A**) of the same figure. Initially, we set an upper bound of 100 cm. Since the parameter values b_4 were close to this upper bound we decided to increase it to 200 cm where we faced the same problem. After increasing it two more times to 400 cm the parameters b_4 were significantly smaller, indicating a successful estimation. The resulting forty estimated lock-in functions are visualized in (**A**) of Figure 7. However, our optimizer found an optimal lock-in function with a half lock-in depth of 262.23 cm, corresponding to an offset of 2745±339 years (mean ± standard deviation with respect to the age depth model). These results are unexpected, as visual inspection of the data suggests a maximum offset of 50 cm.

Table 2. Results overview and some lithostratigraphycal and sedimentological information extracted from the corresponding publications.

Core	$\rho_{0.5}$	ρ_h	ρ_w	Type	Water depth (m)	$\mu_{acc}\pm\sigma_{acc}$[1] (cm/year)	Material[2]
BA3	12.26	0.065	15.43	marine	1431	0.093 ± 0.036	upper part: pervasively bioturbated sediment with a fine-grained texture; lower part: fine-grained, diatom-bearing sediment with coarse bedding
BIR	2.73	1.005	1.14	lacustrine	1.5	0.107 ± 0.049	clay, silty clay
BYE	66.84	0.019	105.31	lacustrine	10.6	0.052 ± 0.008	partly laminated fine detritus gyttja
ByaP2	59.23	0.027	74.58	lacustrine	10.6	0.052 ± 0.008	partly laminated fine detritus gyttja
ByaP3	69.9	0.017	119.76	lacustrine	10.6	0.052 ± 0.008	partly laminated fine detritus gyttja
EIL	1.75	0.728	2.64	lacustrine	6	0.182 ± 0.032	grey to blackish, layered sediments with moderate TIC and TOC contents
FUR	12.23	0.047	41.7	lacustrine	14.2	0.045 ± 0.011	partially laminated fine detritus gyttja/clay gyttja, silt
P2	16.69	0.035	56.98	lacustrine	14.2	0.045 ± 0.011	partially laminated fine detritus gyttja/clay gyttja, silt
P3	0.05	10	0.1	lacustrine	14.2	0.045 ± 0.011	partially laminated fine detritus gyttja/clay gyttja, silt
GYL	38.34	0.015	130.9	lacustrine	17	0.152 ± 0.068	laminated brown fine detritus gyttja
GP1	53.45	0.009	106.9	lacustrine	17	0.152 ± 0.068	laminated brown fine detritus gyttja
GP2	28.99	0.059	29.95	lacustrine	17	0.152 ± 0.068	laminated brown fine detritus gyttja
GP4	32.68	0.029	68.01	lacustrine	17	0.152 ± 0.068	laminated brown fine detritus gyttja
MOR	0.15	3.612	0.45	lacustrine	-	0.036 ± 0.011	clay, silty clay
MST	8.45	0.069	28.87	marine	267	0.107 ± 0.049	-
U1305	11.17	0.055	27.79	marine	3459	0.062 ± 0.016	ranges from silty clay with sand and little biogenic material, to homogenous nannofossil ooze with silty clay and common bioturbation

[1]Mean and standard deviation of accumulation rate derived from our age-depth models.
[2]Information is taken from publications and shortly summarized.
For more detailed information see the original publications.

To investigate this discrepancy, we tried various approaches, including increasing uncertainties, eliminating more data points as outliers, and testing different age-depth models. Nonetheless, these attempts were leading to similar results. After using the E/I-analysis tool on Palaeomagnetism.org 2.4.0 (Jollyfant & Pastor-Galán, 2022; M. R. Koymans et al., 2016; M. Koymans et al., 2020) to remove possible inclination shallowing we obtain meaningful results that agree with visual interpretation and expectation. The E/I-analysis yielded a flattening factor of $f = 0.54$, indicating significant inclination shallowing (see Figure S12, Supporting Information). To remove inclination shallowing we used the following formula proposed by R. King (1955)

$$\tan(I_o) = f \tan(I_f) \tag{7}$$

where I_o is the observed inclination and I_f the inclination of the external field.

Subsequently, we present the results after applying the flattening factor in Figure 8. The analysis highlights the crucial role of diligent data preprocessing and the importance of considering various factors that can impact the final outcomes of our method.

Removed data points: The first 7 data points from the upper part of the record have been removed due to an abrupt decrease in the inclinations. Additionally, three data points at depth 460, 462 and 464 cm were removed as obvious outlier.

Declination offset: The palaeomagnetic data is divided into three sub-sections. The estimated declination offset values are 9.64 ± 1.36 for the upper part, -2.17 ± 2.3 for the middle, and 1.53 ± 1 for the lower part.

Age-depth model: Radiocarbon dates above 700cm were taken from the original publication and used to construct the age-depth model. The original publication suggests applying a local reservoir correction of 500-700 years. We decided to employ a correction of 600 years and include an additional error of 200 years to compensate for uncertainty in the reservoir effect estimation. For two depths, both plant remains (orange in Fig. 8) and bulk samples (blue) were taken, allowing to estimate an additonal reservoir effect of 500 years for the bulk sediment. See the original publication for a discussion of possible mechanisms causing the local reservoir effects.

Estimation: After accounting for inclination shallowing an upper bound of 100 cm turned out to be appropriate. Furthermore, the predicted sediment observations demonstrated a decent correspondence with the actual data, indicating a good fit.

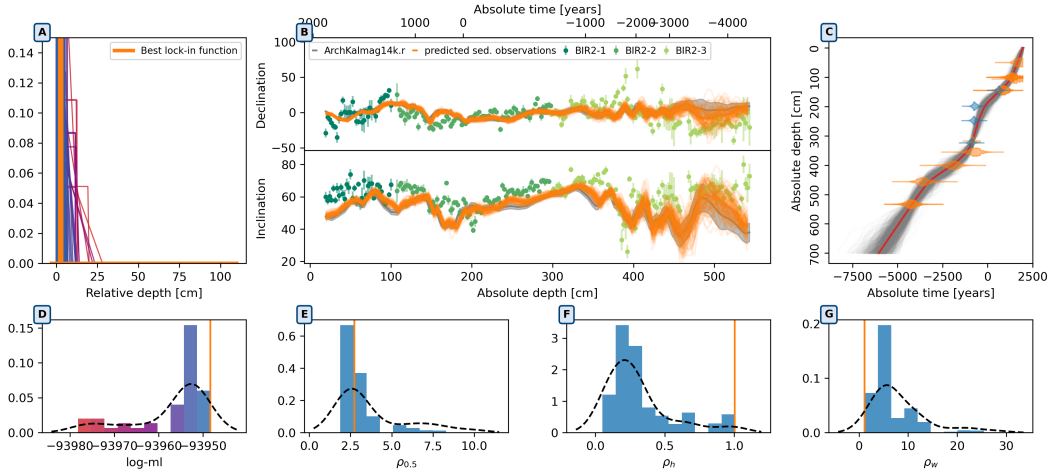

Figure 8. Results for BIR after accounting for inclination shallowing.

4 Discussion

Applying the proposed method to nine sediment records yields insightful results, demonstrating the general occurrence of offsets and smoothed signals induced by the pDRM process. The range of examples spans from records with almost no distortion (EIL, BIR, MOR) to those with offsets of nearly 70 cm and significant smoothing (see BYE and its sub-cores). While the four parameters b_1 to b_4 are not as precisely determined as the half lock-in depth, the last parameter b_4, representing the maximal lock-in depth, remains an intriguing parameter to consider. Estimated results of this parameter range from maximum lock-in depths of only a few centimeters to over 130 cm.

While acknowledging that nine examples are insufficient for comprehensive statistical analysis, the observed pDRM effects in six out of the nine sediment records highlight the significance of accounting for this phenomenon. Most of the half lock-in depths of the six records displaying pDRM effects range from 10 to 20 cm. Notably, examples like GYL and BYE demonstrate the potential occurrence of much higher half lock-in depths, reaching 38 cm and 67 cm. However, it appears that half lock-in depths exceeding 30 cm are less common.

The influence of the number of surrounding archaeomagnetic data on the method, was found to be moderate in synthetic tests (Bohsung et al., 2023). In other words, the estimation works even in areas where archaeomagnetic and volcanic data is sparse. Yet, as exemplified by MOR, it does affect the uncertainties in predicted sediment observations. This is not surprising and related to the fact that the uncertainties decrease with the number of data.

Investigating potential distinctions between marine and lacustrine sediment records is an interesting question. However, with only three marine records in our dataset, a more extensive collection is necessary for a conclusive analysis. Similarly, when it comes to correlating lock-in function parameters with sedimentological or lithostratigraphic features, the current data set remains insufficient for comprehensive examination. Looking ahead, we plan a more detailed and methodical study, aimed at thoroughly exploring these relationships. Our primary focus in this study, though, was to concentrate on the practical application of the newly introduced method across a carefully selected list of sediment records. This initial focus provided a foundation for future, more extensive inquiries. To advance our understanding in these areas, collaboration with experts in sedimentology will be pivotal. Their insights will be instrumental in unraveling the complex interactions and variations inherent in different sedimentary environments.

A notable finding emphasizes the necessity for caution when dealing with sediment records composed of multiple sub-cores. Discrepancies between combined records and sub-cores, exemplified by BYE, FUR, and GYL, emphasize the importance of treating them individually. This recommendation becomes particularly pertinent when significant distances between individual cores may lead to slight variations in sedimentation processes. The individual differences in these cases are discussed in the respective sediment record sections.

5 Conclusion

In this paper we applied the method presented in Bohsung et al. (2023) to analyze nine sediment records from different locations worldwide. The results reveal the presence of distortions associated with the lock-in or pDRM process in six out of the nine investigated sediment records.

In addition to the investigation of the pDRM process, we propose a new method for estimating the offset required to transferring relative to absolute declinations. Our method uses the ArchKalmag14k.r model (Schanner et al., 2022), which relies solely on archaeomagnetic data. The proposed Bayesian modeling technique is able to take uncertainties into account, making the estimated offset more reliable.

The example of BIR underscores the significance of meticulous data preprocessing and the consideration of distortions beyond pDRM that may impact the data. This includes an accurate estimation of absolute declination and the consideration of inclination shallowing.

Motivated by our findings, we will work on involving simultaneous estimation of declination offset parameters and the shallowing factor, along with lock-in function parameters. In other words, we will estimate all parameters related to these effects simultaneously, resulting in a comprehensive sediment data preprocessing software for general applicability.

Furthermore, we will explore the deconvolution and application of the estimated parameters to the sediment data. Our goal is to develop a specialized sediment preprocessing software, enhancing the reliability of sediment data for geomagnetic field modeling.

Open Research Section

All data (except for MST) used in this study as well as a python implementation of the method can be found in the GitLab repository (Bohsung & Schanner, 2023). The data for the MST record is not publically available. The author send us the data but did not agree to publish the raw data. Therefore, we published our results but you will not find it in the repository. To reproduce the results you have to ask the author for the data and then use our preprocessing routine. On our website (https://sec23.git-pages.gfz-potsdam.de/korte/pdrm/) jupyter notebooks have been published that can be used to reconstruct the results presented in this paper or to apply the method to additional data. The raw data for records from GEOMAGIA can be found on GEOMAGIA (Brown et al., 2015). More results can be found in Supporting Information.

Acknowledgments

This work was funded by the Deutsche Forschungsgemeinschaft (DFG, German Research Foundation), grant 388291411. L. Bohsung and M. Schanner performed theoretical and conceptual work, with support of M. Korte and M. Holschneider. The manuscript was assembled by L. Bohsung with support from all co-authors. Software development and data processing was conducted by M. Schanner and L. Bohsung. The work and findings were supervised by M. Korte and M. Holschneider.

The authors wish to thank S. Panovska for constructive and helpful discussions and comments especially with respect to inclination shallowing that improved the quality of this study.

References

Arneitz, P., Egli, R., Leonhardt, R., & Fabian, K. (2019). A Bayesian iterative geomagnetic model with universal data input: Self-consistent spherical harmonic evolution for the geomagnetic field over the last 4000 years. *Physics of the Earth and Planetary Interiors*, *290*, 57–75. doi: 10.1016/j.pepi.2019.03.008

Baerenzung, J., Holschneider, M., Wicht, J., Lesur, V., & Sanchez, S. (2020). The Kalmag model as a candidate for IGRF-13. *Earth, Planets and Space*, *72*, 1–13. doi: 10.1186/s40623-020-01295-y

Béguin, A., Filippidi, A., de Lange, G. J., & de Groot, L. V. (2019). The evolution of the Levantine Iron Age geomagnetic anomaly captured in Mediterranean sediments. *Earth and Planetary Science Letters*, *511*, 55–66. doi: 10.1016/j.epsl.2019.01.021

Blaauw, M., & Christen, J. A. (2011). Flexible paleoclimate age-depth models using an autoregressive gamma process. *Bayesian Analysis*, *6*(3), 457 – 474. Retrieved from `https://doi.org/10.1214/11-BA618` doi: 10.1214/11-BA618

Bohsung, L., & Schanner, M. (2023). *Estimating pDRM effects* [Software]. `https://git.gfz-potsdam.de/sec23/korte/pdrm`. GitLab.

Bohsung, L., Schanner, M., Korte, M., & Holschneider, M. (2023). Estimating post-depositional detrital remanent magnetization (pdrm) effects: A flexible lock-in function approach. *Journal of Geophysical Research: Solid Earth*, *128*(12), e2023JB027373. Retrieved from `https://agupubs.onlinelibrary.wiley.com/doi/abs/10.1029/2023JB027373` (e2023JB027373 2023JB027373) doi: https://doi.org/10.1029/2023JB027373

Brown, M. C., Donadini, F., Nilsson, A., Panovska, S., Frank, U., Korhonen, K., ... Constable, C. G. (2015). GEOMAGIA50. v3: 2. A new paleomagnetic database for lake and marine sediments. *Earth, Planets and Space*, *67*, 1–19. doi: 10.1186/s40623-015-0233-z

Caricchi, C., Lucchi, R. G., Sagnotti, L., Macrì, P., Morigi, C., Melis, R., ... Hanebuth, T. J. (2018). Paleomagnetism and rock magnetism from sediments along a continental shelf-to-slope transect in the NW Barents Sea: Implications for geomagnetic and depositional changes during the past 15 thousand years. *Global and planetary change*, *160*, 10–27. doi: 10.1016/j.gloplacha.2017.11.007

Caricchi, C., Sagnotti, L., Campuzano, S. A., Lucchi, R. G., Macrì, P., Rebesco, M., & Camerlenghi, A. (2020). A refined age calibrated paleosecular variation and relative paleointensity stack for the NW Barents Sea: Implication for geomagnetic field behavior during the Holocene. *Quaternary Science Reviews*, *229*, 106133. doi: 10.1016/j.quascirev.2019.106133

Constable, C., Korte, M., & Panovska, S. (2016). Persistent high paleosecular variation activity in southern hemisphere for at least 10 000 years. *Earth and Planetary Science Letters*, *453*, 78–86. doi: 10.1016/j.epsl.2016.08.015

Egli, R., & Zhao, X. (2015). Natural remanent magnetization acquisition in bioturbated sediment: General theory and implications for relative paleointensity reconstructions. *Geochemistry, Geophysics, Geosystems*, *16*(4), 995–1016.

Felden, J., Möller, L., Schindler, U., Huber, R., Schumacher, S., Koppe, R., ... Glöckner, F. O. (2023). PANGAEA-Data Publisher for Earth & Environmental Science. *Scientific Data*, *10*(1), 347.

Frank, U., Schwab, M. J., & Negendank, J. F. (2002). A lacustrine record of paleomagnetic secular variations from Birkat Ram, Golan Heights (Israel) for the last 4400 years. *Physics of the Earth and Planetary Interiors*, *133*(1-4), 21–34. doi: 10.1016/S0031-9201(02)00085-7

Frank, U., Schwab, M. J., & Negendank, J. F. (2003). Results of rock magnetic investigations and relative paleointensity determinations on lacustrine sediments from Birkat Ram, Golan Heights (Israel). *Journal of Geophysical Research: Solid Earth*, *108*(B8). doi: 10.1029/2002JB002049

Gogorza, C., Sinito, A., Tommaso, I., Vilas, J., Creer, K., & Nuñez, H. (2000). Geomagnetic secular variations 0–12 kyr as recorded by sediments from Lake Moreno (southern Argentina). *Journal of South American Earth Sciences*, *13*(7), 627–645. doi: 10.1016/S0895-9811(00)00052-3

Griffiths, D., King, R., Rees, A., & Wright, A. E. (1960). The remanent magnetism of some recent varved sediments. *Proceedings of the Royal Society of London. Series A. Mathematical and Physical Sciences*, *256*(1286), 359–383. doi: 10.1098/rspa.1960.0113

Hamano, Y. (1980). An experiment on the post-depositional remanent magnetization in artificial and natural sediments. *Earth and Planetary Science Letters*, *51*(1), 221–232.

Heaton, T. J., Köhler, P., Butzin, M., Bard, E., Reimer, R. W., Austin, W. E. N., ... et al. (2020). Marine20—The Marine Radiocarbon Age Calibration Curve (0–55,000 cal BP). *Radiocarbon*, *62*(4), 779–820. doi: 10.1017/RDC.2020.68

Hellio, G., & Gillet, N. (2018). Time-correlation-based regression of the geomagnetic field from archeological and sediment records. *Geophysical Journal Inter-*

national, *214*(3), 1585–1607. doi: 10.1093/GJI/GGY214

Hogg, A. G., Heaton, T. J., Hua, Q., Palmer, J. G., Turney, C. S., Southon, J., ... et al. (2020). SHCal20 Southern Hemisphere Calibration, 0–55,000 Years cal BP. *Radiocarbon*, *62*(4), 759–778. doi: 10.1017/RDC.2020.59

Irving, E. (1957). III. The origin of the palaeomagnetism of the Torridonian sandstones of North-West Scotland. *Philosophical Transactions of the Royal Society of London. Series A, Mathematical and Physical Sciences*, *250*(974), 100–110. doi: 10.1098/rsta.1957.0014

Irving, E., & Major, A. (1964). Post-depositional detrital remanent magnetization in a synthetic sediment. *Sedimentology*, *3*(2), 135–143.

Jollyfant, & Pastor-Galán, D. (2022, Mar). *Jollyfant/PMAG2: v2.4.0.* Zenodo. doi: 10.5281/zenodo.6380888

Kalman, R. E. (1960, 03). A New Approach to Linear Filtering and Prediction Problems. *Journal of Basic Engineering*, *82*(1), 35-45. doi: 10.1115/1.3662552

Katari, K., Tauxe, L., & King, J. (2000). A reassessment of post-depositional remanent magnetism: preliminary experiments with natural sediments. *Earth and Planetary Science Letters*, *183*(1-2), 147–160.

Kent, D. V. (1973). Post-depositional remanent magnetisation in deep-sea sediment. *Nature*, *246*(5427), 32–34.

Khokhlov, A., & Hulot, G. (2016). Principal component analysis of palaeomagnetic directions: converting a Maximum Angular Deviation (MAD) into an $\alpha 95$ angle. *Geophysical Journal International*, *204*(1), 274–291. doi: 10.1093/gji/ggv451

King, D. E. (2009). Dlib-ml: A machine learning toolkit. *The Journal of Machine Learning Research*, *10*, 1755–1758.

King, R. (1955). The remanent magnetism of artificially deposited sediments. *Geophysical Supplements to the Monthly Notices of the Royal Astronomical Society*, *7*(3), 115–134. doi: 10.1111/j.1365-246X.1955.tb06558.x

Koymans, M., van Hinsbergen, D., Pastor-Galán, D., Vaes, B., & Langereis, C. (2020). Towards FAIR paleomagnetic data management through Paleomagnetism. org 2.0. *Geochemistry, Geophysics, Geosystems*, *21*(2), e2019GC008838. doi: 10.1029/2019GC008838

Koymans, M. R., Langereis, C. G., Pastor-Galán, D., & van Hinsbergen, D. J. (2016). *Paleomagnetism. org: An online multi-platform open source environment for paleomagnetic data analysis.* Elsevier. doi: 10.1016/j.cageo.2016.05.007

Lanos, P., Le Goff, M., Kovacheva, M., & Schnepp, E. (2005). Hierarchical modelling of archaeomagnetic data and curve estimation by moving average technique. *Geophysical Journal International*, *160*(2), 440–476. doi: 10.1111/j.1365-246X.2005.02490.x

Malherbe, C., & Vayatis, N. (2017). Global optimization of Lipschitz functions. In *International conference on machine learning* (pp. 2314–2323). doi: 10.48550/arXiv.1703.02628

McNish, A., & Johnson, E. (1938). Magnetization of unmetamorphosed varves and marine sediments. *Terrestrial Magnetism and Atmospheric Electricity*, *43*(4), 401–407. doi: 10.1029/TE043i004p00401

Mellström, A., Muscheler, R., Snowball, I., Ning, W., & Haltia, E. (2013). Radiocarbon wiggle-match dating of bulk sediments—how accurate can it be? *Radiocarbon*, *55*(3), 1173–1186. doi: 10.1017/S0033822200048086

Nilsson, A., Holme, R., Korte, M., Suttie, N., & Hill, M. (2014). Reconstructing Holocene geomagnetic field variation: new methods, models and implications. *Geophysical Journal International*, *198*(1), 229–248. doi: 10.1093/gji/ggu120

Nilsson, A., & Suttie, N. (2021). Probabilistic approach to geomagnetic field modelling of data with age uncertainties and post-depositional magneti-

sations. *Physics of the Earth and Planetary Interiors*, *317*, 106737. doi: 10.1016/j.pepi.2021.106737

Otofuji, Y.-i., & Sasajima, S. (1981). A magnetization process of sediments: laboratory experiments on post-depositional remanent magnetization. *Geophysical Journal International*, *66*(2), 241–259.

Panovska, S., Korte, M., Finlay, C., & Constable, C. (2015). Limitations in paleomagnetic data and modelling techniques and their impact on Holocene geomagnetic field models. *Geophysical Journal International*, *202*(1), 402–418. doi: 10.1093/gji/ggv137

Rasmussen, C. E. (2004). Gaussian Processes in Machine Learning. In O. Bousquet, U. von Luxburg, & G. Rätsch (Eds.), *Advanced lectures on machine learning: Ml summer schools 2003, canberra, australia, february 2 - 14, 2003, tübingen, germany, august 4 - 16, 2003, revised lectures* (pp. 63–71). Berlin, Heidelberg: Springer Berlin Heidelberg. doi: 10.1007/978-3-540-28650-9_4

Reimer, P. J., Austin, W. E. N., Bard, E., Bayliss, A., Blackwell, P. G., Bronk Ramsey, C., ... et al. (2020). The IntCal20 Northern Hemisphere Radiocarbon Age Calibration Curve (0–55 cal kBP). *Radiocarbon*, *62*(4), 725–757. doi: 10.1017/RDC.2020.41

Roberts, A. P., & Winklhofer, M. (2004). Why are geomagnetic excursions not always recorded in sediments? Constraints from post-depositional remanent magnetization lock-in modelling. *Earth and Planetary Science Letters*, *227*(3-4), 345–359. doi: 10.1016/j.epsl.2004.07.040

Schanner, M., Korte, M., & Holschneider, M. (2022). ArchKalmag14k: A Kalman-Filter Based Global Geomagnetic Model for the Holocene. *Journal of Geophysical Research: Solid Earth*, *127*(2), e2021JB023166. doi: 10.1029/2021JB023166

Schwab, M. J., Neumann, F., Litt, T., Negendank, J. F., & Stein, M. (2004). Holocene palaeoecology of the Golan Heights (Near East): investigation of lacustrine sediments from Birkat Ram crater lake. *Quaternary Science Reviews*, *23*(16-17), 1723–1731. doi: 10.1016/j.quascirev.2004.05.001

Snowball, I., Mellström, A., Ahlstrand, E., Haltia, E., Nilsson, A., Ning, W., ... Brauer, A. (2013). An estimate of post-depositional remanent magnetization lock-in depth in organic rich varved lake sediments. *Global and planetary change*, *110*, 264–277. doi: 10.1016/j.gloplacha.2013.10.005

Snowball, I., & Sandgren, P. (2004). Geomagnetic field intensity changes in Sweden between 9000 and 450 cal BP: extending the record of "archaeomagnetic jerks" by means of lake sediments and the pseudo-Thellier technique. *Earth and Planetary Science Letters*, *227*(3-4), 361–376. doi: 10.1016/j.epsl.2004.09.017

Stacey, F. (2012). *The physical principles of rock magnetism* (No. 5). Elsevier.

Stoner, J. S., Channell, J. E., Mazaud, A., Strano, S. E., & Xuan, C. (2013a). The influence of high-latitude flux lobes on the Holocene paleomagnetic record of IODP Site U1305 and the northern North Atlantic. *Geochemistry, Geophysics, Geosystems*, *14*(10), 4623–4646. doi: 10.1002/ggge.20272

Stoner, J. S., Channell, J. E., Mazaud, A., Strano, S. E., & Xuan, C. (2013b). *NOAAWDS Paleoclimatology - Paleomagnetic Data from IODP Site U1305 and the Northern North Atlantic During the Holocene* [Data]. NOAA National Centers for Environmental Information. doi: 10.25921/ffzn-jb18

Suganuma, Y., Okuno, J., Heslop, D., Roberts, A. P., Yamazaki, T., & Yokoyama, Y. (2011). Post-depositional remanent magnetization lock-in for marine sediments deduced from 10Be and paleomagnetic records through the Matuyama–Brunhes boundary. *Earth and Planetary Science Letters*, *311*(1-2), 39–52. doi: 10.1016/j.epsl.2011.08.038

Suttie, N., & Nilsson, A. (2019). Archaeomagnetic data: The propagation of an error. *Physics of the Earth and Planetary Interiors*, *289*, 73–74. doi: 10.1016/j.pepi.2019.02.008

Verosub, K. L. (1977). Depositional and postdepositional processes in the magnetization of sediments. *Reviews of Geophysics*, *15*(2), 129–143. doi: 10.1029/RG015i002p00129

Wündsch, M., Haberzettl, T., Meadows, M. E., Kirsten, K. L., Kasper, T., Baade, J., ... Mäusbacher, R. (2016). The impact of changing reservoir effects on the 14C chronology of a Holocene sediment record from South Africa. *Quaternary Geochronology*, *36*, 148–160. doi: 10.1016/j.quageo.2016.08.011

Wündsch, M., Haberzettl, T., Meadows, M. E., Kirsten, K. L., Kasper, T., Baade, J., ... Mäusbacher, R. (2016). Palaeomagnetic data of sediment core EV13 from coastal lake Eilandvlei, southern Cape coast, South Africa [data set]. PANGAEA. Retrieved from `https://doi.org/10.1594/PANGAEA.867928` (In supplement to: Wündsch, M et al. (2016): The impact of changing reservoir effects on the 14C chronology of a Holocene sediment record from South Africa. Quaternary Geochronology, 36, 148-160, https://doi.org/10.1016/j.quageo.2016.08.011) doi: 10.1594/PANGAEA.867928

Zillén, L., Snowball, I., Sandgren, P., & Stanton, T. (2003). Occurrence of varved lake sediment sequences in Varmland, west central Sweden: lake characteristics, varve chronology and AMS radiocarbon dating. *Boreas*, *32*(4), 612–626. doi: 10.1080/03009480310004189

Zillén, L. M., Wastegård, S., & Snowball, I. F. (2002). Calendar year ages of three mid-Holocene tephra layers identified in varved lake sediments in west central Sweden. *Quaternary Science Reviews*, *21*(14-15), 1583–1591. doi: 10.1016/S0277-3791(02)00036-7